VLA observations of 43 GHz continuum and CS J=1–0 emission from Orion-IRc2 and the hot core

Claire J. Chandler
Mullard Radio Astronomy Observatory, Cavendish Laboratory, Madingley Road, Cambridge CB3 0HE, United Kingdom

and

Douglas O. S. Wood
Eastman Kodak, Scientific Imaging Systems, 4 Science Park, New Haven, CT 06511, USA

ABSTRACT

We have used the VLA to image at 2″ resolution the Orion-IRc2 region in 43 GHz continuum and CS(1–0) emission. In the continuum radio sources I and B are detected together with an extended emission component which peaks at source I. Comparison of this extended component with lower frequency data suggests it is free-free emission from a dusty HII region ionized by source I. The compact CS(1–0) emission originates from the hot core, the compact ridge, and the western clump. The hot core component has a line brightness temperature of ~ 150 K, and is optically thick. We derive an abundance for the CS relative to H_2 in the hot core of 1.2×10^{-8}, considerably higher than the previous upper limit based on a single-dish spectral line survey. The difference can be explained as being due to beam-dilution of the hot core component in the earlier, low-resolution study, and the confusion of the hot core with emission from the extended ridge. A similar result is also suggested for the sulphur-bearing molecules SO and SO_2, and existing models of sulphur chemistry are unable to reproduce these new abundance estimates. We conclude that models extending to higher temperatures and densities are required to explain these data.

Subject headings: ISM: abundances — ISM: molecules — ISM: individual: Orion-IRc2 — HII regions — Radio lines: molecular: interstellar

1. Introduction

The Orion-IRc2 region is the nearest example of high-mass star formation ($D = 450$ pc: Anthony-Twarog 1982) and therefore one of the most important sites in which to investigate the small-scale dynamics of the star formation process, and its affect on the surrounding interstellar medium at high spatial resolution. A large number of studies have revealed a wealth of activity around the Becklin-Neugebauer (BN) object and the infrared sources IRc2–7 (see Genzel & Stutzki 1989 for a review). Initially low-resolution, single-dish observations were used to identify several different spectral components in molecular line emission, all of which show distinct velocity structure and chemistry. Subsequent high-resolution interferometric imaging has revealed the spatial structures corresponding to these spectral components (e.g., Wright, Plambeck & Wilner 1996 and references therein). Most of the activity is centred on the compact radio source "I," which displays an energetic outflow (Masson et al. 1987; Chernin & Wright 1996), a rotating ring of SiO masers (Plambeck, Wright & Carlstrom 1990; Menten & Reid 1995), and high-velocity H_2O and OH masers (Genzel et al. 1981; Hansen & Johnston 1983).

Two arcseconds to the southeast of source I is the "hot core," where the emission from dust and many molecules peaks (Masson et al. 1985; Wright & Vogel 1985; Masson & Mundy 1988; Migenes et al. 1989; Murata et al. 1992; Wright et al. 1996). Temperatures of 200–300 K are measured at the hot core (Hermsen et al. 1988b; Wilner, Wright & Plambeck 1994), and nitrogen-bearing species are particularly abundant at this location due to high-temperature grain chemistry (Caselli, Hasegawa & Herbst 1993). To the south and west of the hot core is a compact ridge 10–15$''$ in extent in which many oxygen-rich molecules are detected, indicating a chemistry entirely different from the hot core (Blake et al. 1987).

The single-dish molecular line study and chemical modelling of the different spectral components carried out by Blake et al. (1987) indicated that the sulphur compounds SO, SO_2, and CS reside mainly in the "plateau," or high-velocity outflow component, and in the extended cloud, but not in the hot core or compact ridge. However, high-resolution images of the SO and SO_2 emission (Wright et al. 1996) indicate that both molecules *are* associated with the hot core, and are also located in a shell-like structure surrounding the plateau region. We therefore decided to make use of the new high-frequency capability of the VLA to image CS(1–0) in Orion-IRc2 with 2$''$ resolution, to examine its relationship to the emission from other sulphur-bearing molecules, and to investigate the small-scale kinematics of the dense gas. We find that, like the SO and SO_2, CS emission is also strong at the hot core, and conclude that the hot core component was too beam diluted and confused by emission from the extended ridge to have been identified as a separate component in earlier studies. We have also obtained a 2$''$ resolution continuum image of IRc2 at 43 GHz, a frequency where both dust and ionized gas are expected to contribute to the emission.

2. Observations and data reduction

Observations of IRc2 in 43 GHz continuum emission were made on 1994 November 22 using the inner 10 antennas of the Very Large Array (VLA) of the National Radio Astronomy Observatory[1] in C configuration. One IF with a 0.78 MHz (5.4 km s^{-1}) continuum channel was centered on the SiO v=1 J=1–0 maser feature at 43.122 GHz, $V_{\rm LSR}$ = -3.8 km s^{-1} (see Menten & Reid 1995), to monitor the atmospheric phase fluctuations on 10-second time intervals. A second IF with a continuum channel of 50 MHz bandwidth was centered at 43.3 GHz, away from any line emission. Right and left circular polarizations were measured at both frequencies. The quasar 0605$-$085 was observed every half an hour to monitor instrumental phase offsets between the two IFs. The position of the -3.8 km s^{-1} maser feature using 0605$-$085 as the phase reference was found to be $\alpha(1950) = 05^{\rm h}\ 32^{\rm m}\ 47\overset{\rm s}{.}028$, $\delta(1950) = -05^\circ\ 24'\ 23\overset{''}{.}81$, which is within $0\overset{''}{.}2$ (one tenth of our synthesized beam) of that measured by Menten & Reid (1995). Solutions for the complex gain were obtained every 10 seconds from the SiO maser data, and applied to the 50 MHz continuum channel. The absolute calibration was obtained from 3C48, with an assumed flux density of 0.53 Jy at 43 GHz. This gives a flux density for 0605$-$085 of 2.00 $\pm$ 0.11 Jy, and for the -3.8 km s^{-1} maser feature in a 0.78 MHz bandwidth of 761 $\pm$ 26 Jy. The data were calibrated and imaged using the AIPS reduction package. The synthesized beam, which is intermediate between uniform and natural weighting ("robust" weighting: Briggs 1995), is optimized for a combination of resolution and sensitivity, and has $\theta_{\rm B} = 2\overset{''}{.}38 \times 1\overset{''}{.}87$ at P.A. -60°. The rms noise in the final image is 0.53 mJy (equivalent to 78 mK for the above $\theta_{\rm B}$).

The CS J=1–0 line at 48.991 GHz was observed on 1994 November 18 using the 10 VLA antennas equipped with 40–50 GHz receivers, also in C configuration. One IF with right circular polarization was observed using 64 channels of 195 kHz (1.2 km s^{-1}) resolution, centered at $V_{\rm LSR}$ = 7.0 km s^{-1}. The atmospheric and instrumental phase was monitored by observing 0605$-$085 every 10 minutes, and 0605$-$085 was also used to measure the bandpass after smoothing with a boxcar over 4 channels. The zenith opacity at 49 GHz, which was obtained from tipping scans using all 10 antennas, was approximately 0.15, about a factor of 2 higher than that commonly measured at 43 GHz. Absolute calibration was achieved from observations of 3C286, with an assumed flux density extrapolated from lower frequencies of 1.32 Jy. This gives a flux density for 0605$-$085 at 49 GHz of 2.59 $\pm$ 0.08 Jy. The uv data were calibrated, imaged, and CLEANed using routines in AIPS. The

[1]The National Radio Astronomy Observatory is a facility of the National Science Foundation operated under cooperative agreement by Associated Universities, Inc.

synthesized beam with robust weighting is $2\farcs11 \times 1\farcs69$ at PA $-46°$, and the rms noise in each 1.2 km s^{-1} channel is 33 mJy (4.7 K). We estimate that the uncertainty in the absolute flux density scale is $\sim 15\%$ at both 43 and 49 GHz. All images have been corrected for the reponse of the primary beam, so the noise level is not uniform across the field. The largest angular size scale which is Nyquist-sampled by the observations is approximately $10''$.

3. Results

3.1. Continuum emission

The 43 GHz continuum emission from the Orion-IRc2 region is displayed in Figure 1, in which the positions of radio sources B, I, and "n" (Menten & Reid 1995) are marked as triangles. Unresolved emission is associated with both B and I at 43 GHz. Structure is also observed extending to the southwest of source I. Large-scale emission from the foreground HII region results in the prominent negative features when using CLEAN deconvolution, and makes source B sit in a negative bowl. In order to estimate the flux density of the unresolved sources it is therefore necessary to image only those data with projected baselines longer than 40 kλ (i.e., remove all structure on angular scales $\theta > 2.5''$). The resulting image is shown in Figure 2a. This analysis gives flux densities and upper limits to the FWHM source sizes of 28.0 ± 0.6 mJy, $\theta_{\rm S} \lesssim 0\farcs6$ for source B, and 10.8 ± 0.6 mJy, $\theta_{\rm S} \lesssim 0\farcs7$ for source I. These are in excellent agreement with the 43 GHz flux densities reported by Menten & Reid (1995), which were obtained in the VLA A-array with a $0\farcs25$ synthesised beam. Plambeck et al. (1995) show that the emission from source I, $S \propto \nu^{1.5}$, is consistent with arising from an HII region, or a combination of an HII region and a dusty disk.

After subtracting point sources at the positions of B and I the structure of the remaining extended emission is displayed in Figure 2b. Unlike the 86 GHz and 218 GHz continuum (Plambeck et al. 1995; Wright et al. 1996; Blake et al. 1996) the extended 43 GHz emission peaks at the position of source I, rather than the hot core, with a flux density of 8 mJy beam^{-1}. A second 8 mJy peak is located $1''$ to the southeast of radio source n. To obtain limits on the contribution we expect from dust in the hot core at 43 GHz, we scale the flux densities obtained at 86 GHz in a $1\farcs67 \times 0\farcs76$ beam (Plambeck et al. 1995) and at 98 GHz in a $3\farcs3 \times 2\farcs2$ beam (Murata et al. 1992) by a ν^2 dust opacity (Wright et al. 1992). Extrapolating from the 86 GHz measurement gives a predicted 43 GHz flux density of 3 mJy, while the 98 GHz value predicts 8 mJy. The 218 GHz flux density observed in a $2\farcs1 \times 1\farcs5$ beam by Blake et al. (1996) predicts a lower limit of 1.3 mJy at 43 GHz, and so does not provide a firmer constraint on the expected contribution from dust; it is likely that these higher-frequency measurements resolve out more of the extended emission than at λ 3 mm and λ 7 mm. At the position of the peak CS(1–0) emission (§ 3.2), which we associate with the hot core, we find a 43 GHz flux density of 6 mJy beam^{-1}, comfortably within the range predicted by the higher frequency data. The source detected to the west of I at 43 GHz does not coincide with any of the continuum emission peaks observed at higher frequencies (Wright et al. 1992; Murata et al. 1992; Plambeck et al. 1995). A second extended emission component besides the hot core is clearly needed to explain the structure observed at 43 GHz. The nature of this component is discussed in § 4.1 below.

3.2. CS(1–0) emission

Emission in CS(1–0) is detected in the 1.2 km s^{-1} wide channels at the 6σ level or higher between $V_{\rm LSR} = -2.0$ km s^{-1} and 13.6 km s^{-1}. A map of the CS(1–0) integrated between these velocities is shown in Figure 3. The emission is concentrated in the hot core, $2''$ south and east of source I, in the compact ridge, to the south of source n, and in the "western clump" (e.g., Masson & Mundy 1988), north and west of sources I and n. As was also found in high-resolution ammonia maps (Pauls et al. 1983; Hermsen, Wilson & Bieging 1988a; Migenes et al. 1989), no CS(1–0) is associated with source B. This supports the idea proposed by Plambeck et al. (1995) that BN is not associated with the molecular cloud, but lies along the line of sight to the IRc2 region by chance. A comparison of the emission in Figure 3 with the single-dish measurements reported by Hasegawa et al. (1984) and Tatematsu et al. (1993) shows that only 15–20% of the total CS(1–0) flux density is detected by the interferometer. This is consistent with most of the CS emission originating in the extended molecular cloud (Blake et al. 1987).

The 43 GHz continuum and integrated CS(1–0) emission are not well correlated spatially (Figure 3), but the CS peak at the hot core, $2''$ from source I, coincides well with other molecular species that have been imaged at high resolution such as NH_3 (Migenes et al. 1989), $H^{13}CN$, and SO_2 (Wright et al. 1996). Unlike the nitrogen-rich species, however, the CS also exhibits strong emission from the compact ridge, where oxygen-bearing molecules such as OCS, CH_3OH, and H_2CO are located (Wright et al. 1996; Mangum, Wootten & Plambeck 1993). The western clump is detected in most species, including dust continuum (Wright et al. 1992).

In individual spectral channels the CS emission is observed to comprise distinct compact clumps, each of which can be identified in several consecutive channels (see Figure 4). Gaussian fits to the sources in each channel map lead to the identification of six distinct clumps. The mean positions and deconvolved sizes of these clumps are listed in Table 1;

the typical uncertainty in the derived FWHM of the clumps is $0\farcs5$ to $1''$. The positions are also marked as crosses in Figure 5, which shows a contour plot of peak beam-averaged brightness temperature, T_B. Clumps 1, 2 and 6 have nearby ammonia peaks identified by Migenes et al. (1989). The maximum value of T_B in the CS(1–0) data set is 89 K, and is associated with clump 1, in the 4.6 km s^{-1} channel. For the deconvolved size of clump 1 given in Table 1, this gives a lower limit to the line brightness temperature, T_L, of $\sim$ 150 K, similar to the rotation temperature of NH_3 of 160 K derived for the hot core by Hermsen et al. (1988b).

Spectra of the individual CS clumps are also displayed in Figure 5. The LSR velocities and FWHM line widths obtained from single Gaussian fits to these spectra are given in Table 1. The spectra show that clumps 1 and 2 correspond to the single-dish hot core component, with $V_{\rm LSR} \sim 5$ km s^{-1}, and line width $\Delta V \sim$ 5–8 km s^{-1} (see, e.g., Blake et al. 1987 for a summary of the single-dish components). Clumps 3 and 4 have similar velocities and line widths to the "compact ridge," with $V_{\rm LSR} \sim$ 7–8 km s^{-1} and $\Delta V \sim$ 3–5 km s^{-1}. Clump 5, which appears to be part of a filament connecting the hot core and the western clump in the integrated CS(1–0) map (Figure 3), has a spectrum which is not at all Gaussian. A comparison with spectra at clump 6 suggests that the systemic velocity of the filament is $\sim$ 6.5 km s^{-1}, and that the asymmetry of the line is caused by a broad, blueshifted wing. Clump 5 lies close to a high-velocity, blueshifted CO(1–0) feature associated with the outflow from source I (Chernin & Wright 1996), and may represent the interaction of the outflow with nearby, dense gas.

The spectrum of clump 6, the western clump, comprises two features. One corresponds to the 6.5 km s^{-1} filament, and is spatially aligned with the filament (see Figure 4). The second component is at a similar velocity to the clump detected in HC_3N by Masson & Mundy (1988), at $\sim$ 12 km s^{-1}. It is less compact than the 6.5 km s^{-1} feature, and extends to the south of clump 6. While the 6.5 km s^{-1} component is quite narrow, $\Delta V \sim 2$ km s^{-1}, the 12 km s^{-1} component is rather broad, $\Delta V \sim 5$ km s^{-1}, and even shows some evidence of a redshifted wing (Figure 5). Alternatively, it is possible that these two spectral components are caused by large-scale emission associated with the molecular cloud at 9 km s^{-1} being too extended and optically-thick to be detected by the interferometer. However, there is little evidence for a similar problem at the positions of the other clumps.

The highest velocity CS(1–0) emission detected is associated with source I. Figure 6 shows the redshifted emission integrated between $V_{\rm LSR} = 20.7$ and 32.7 km s^{-1}, located to the east of source I, and the blueshifted emission between -13.9 and -2.0 km s^{-1}, with a peak at the position of the radio source and a feature extending to the west. In order to estimate the contribution from the continuum to the features in Figure 6 we extrapolate our 43 GHz continuum flux densities to 49 GHz using the spectral indices measured by Plambeck et al. (1995) for sources I and B. We estimate that the 49 GHz continuum contributes $\leq$ 27 mJy beam^{-1} and $\approx$ 33 mJy beam^{-1} for I and B respectively. Thus the (2 σ) contour in Figure 6 at the position of B is continuum emission, while $>$ 70% of the flux density at source I in the blueshifted CS(1–0) image is molecular line emission. A comparison of Figure 6 with the high-velocity v=0, J=2–1 SiO emission (Wright et al. 1995), which traces the outflow from I, shows good agreement between the two molecules. Furthermore, it is possible that the CS feature to the southwest of source I corresponds to the "bow tie" observed in SiO; higher signal-to-noise ratio observations are needed to confirm this result. A more general comparison between our high-velocity CS(1–0) maps and those of other molecular lines (Wright et al. 1996) confirms the east-west orientation of the outflow. The difference between the CS(1–0) and other high-density tracers, however, is the detection of compact, high-velocity, blueshifted emission, coincident with I, with no redshifted counterpart. This feature appears to be resolved with a source size of $\sim 1\farcs5 \times 1''$ at $\sim 50^{\circ}$, aligned with the SiO maser disk (Plambeck et al. 1990) and the SiO bow tie (Chandler & De Pree 1995; Wright et al. 1995). It may indicate a significant molecular component to the disk, and a contribution to the single-dish plateau feature from rotation, especially at the lower velocities, as well as outflow. It is not clear why a similar redshifted component is not detected.

The peak of the integrated CS(1–0) emission (Figure 3) does not coincide with any of the clumps identified in the spectral channels and which are apparent in Figure 5. Rather, the peak is located between clumps 1 and 2, where the velocity dispersion is highest, and the integrated flux is dominated by the line width rather than the peak intensity. Clump 1 has a millimetre continuum counterpart in the high-resolution images of Plambeck et al. (1995), although in dust emission the peak is closer to I than in CS(1–0), probably because of the different temperature dependence of the dust optical depth ($\tau_{\rm d} \propto N({\rm H_2})$) compared to the CS optical depth ($\tau_{\rm CS} \propto N({\rm H_2})/T_{\rm ex}^2$). Figure 4 shows that clump 2 is a separate feature with a somewhat broader line width than clump 1. It is the location where emission from both these features overlaps along the line of sight, close to clump 2, where the integrated CS emission is a maximum. Only clumps 4 and 6 correspond to local peaks in the velocity dispersion. The line widths of the other clumps may be determined more by the proximity to source I and its outflow.

The intensity-weighted mean $V_{\rm LSR}$ velocity, or first moment, of the CS(1–0) emission (Figure 7) also shows interesting features. There exists a smooth velocity gradient along the ridge connecting clumps 1–4, and along the filament from the hot core to clump 5. The 12 km s^{-1} component of the western clump on the other hand dominates the velocity structure south of clump 6, and results in an average velocity considerably redshifted compared to the bulk of the dense gas. The anticorrelation between the CS(1–0) and near- and mid-infrared emission at this location (e.g., Gezari 1992; Dougados et al. 1993) indicates that even though its velocity is redshifted the molecular material is nevertheless located in front of the infrared nebula rather than behind it.

4. Discussion

4.1. 43 GHz continuum emission – an HII region ionized by source I?

The first possibility we have investigated for the origin of the extended continuum emission observed at 43 GHz (Figure 2b) is the contamination of our 50 MHz continuum channel by molecular line emission. Using the spectral line catalogue of Poynter & Pickett (1985), we have calculated the line strengths for the molecules detected in the hot core, the plateau, and the compact ridge by Blake et al. (1987) assuming a temperature of 160 K. We estimate that a maximum contribution of 1 mJy integrated over the central 30″ can arise from the molecules C_2H_5OH, HCOOH, CH_3OCH_3, C_2H_5CN, CH_3OCHO and SO_2. We therefore conclude that the extended structure is not due to molecular lines in our bandpass.

In order to examine whether the extended structure could be free-free emission we have compared it with 22.5 GHz continuum data obtained using the VLA in D configuration, kindly provided by L. Mundy. There are clearly emission peaks in the 22 GHz map which coincide with features observed at 43 GHz, including maxima close to sources I and n as well as source B. To compare directly the flux densities in these components at the two frequencies we have attempted to match the *uv* coverage in the two data sets by applying an inner 8 kλ cut-off to the 22 GHz data to match the smallest spatial frequency measured at 43 GHz, resulting in a synthesised CLEAN beam of $3''.03 \times 2''.54$, and then by smoothing the 43 GHz map to this same resolution. The mean spectral index α ($S \propto \nu^{\alpha}$) over a region of the map where the signal-to-noise ratio at both frequencies is greater than 3 is then 1.1 ± 0.5. This rules out dust as the origin of the extended component, and suggests that the emission mechanism is thermal bremsstrahlung, either from an HII region ionized by source I or from an ionized wind.

The orientation of the extended emission centred on source I is not the same as the bow tie observed in SiO emission (Plambeck et al. 1990; Chandler & De Pree 1995; Wright et al. 1995), and so is unlikely to be associated with the molecular disk or the photo-ionization of the disk surface by source I (e.g., Hollenbach et al. 1994). It tends to lie along the edge of, and is anti-correlated with, the dense molecular gas traced by the integrated CS(1–0) emission. This indicates that it may represent the photo-ionization of the surface of the hot core, the compact ridge, and the western clump by source I. It fits the recent picture suggested by Blake et al. (1996) in which strong excitation gradients exist in the hot core, with the highest energy density located on the side closest to source I, and cooler material residing at larger distances from I; the ionized gas represents the most extreme conditions.

The peak brightness temperature in the extended emission is 1.2 K, implying a peak optical depth of 1.2×10^{-4}, assuming an electron temperature of 10^4 K. This gives an emission measure of 10^6 pc cm^{-6}, and an electron density of 1.5×10^4 cm^{-3} (Mezger & Henderson 1967). Integrated over the nebula the observed flux density is 79 ± 3 mJy, implying a Lyman continuum photon rate of 9×10^{44} s^{-1} which could be produced by a B1 ZAMS star with a luminosity $\approx 5 \times 10^3$ $L_\odot$. Since this luminosity is an order of magnitude lower than that needed to power the Kleinmann-Low nebula (Downes et al. 1981) it is most likely that the ionized gas has a significant dust content absorbing the UV photons.

4.2. CS in the hot core

In an extensive single-dish survey of molecules in the Orion-IRc2 region Blake et al. (1987) found no evidence of sulphur-bearing molecules in the hot core, including an upper limit on the CS abundance relative to H_2 of $\lesssim 5 \times 10^{-10}$. With the higher resolution available with aperture synthesis techniques, however, we find that most of the *compact* CS emission is associated with the hot core (clumps 1 and 2 in Figure 5). The integrated flux in this component is 15 Jy km s^{-1}, and we use this to calculate the abundance of CS in the hot core in the following manner. From the spectral decomposition performed by Blake et al., the column density of CO in the hot core component, averaged over their $30''$ beam, is 1.0×10^{19} cm^{-2}. Assuming $T_{\rm ex} = 160$ K (Hermsen et al. 1988b), LTE, and $\tau = -\ln(1 - T_R/T_{\rm ex}) \approx 0.5$ for the $T_R \approx 60$ K observed in the CS(1–0) line (Figure 5), we find that the integrated CS flux corresponds to a CS column density of 1.0×10^{15} cm^{-2} when averaged over an $\approx 30''$ beam. The abundance of CS relative to molecular hydrogen is then found from $X(\mathrm{CS}) = N(\mathrm{CS})/N(\mathrm{CO}) \times X(\mathrm{CO})$, where $X(\mathrm{CO}) = 1.2 \times 10^{-4}$ for the hot core (Blake et al. 1987), and gives $X(\mathrm{CS}) = 1.2 \times 10^{-8}$. This is clearly considerably higher than the upper limit obtained by Blake et al. for the hot core, but lies between the abundances found for the plateau (2.2×10^{-8}) and the extended ridge (2.5×10^{-9}).

To investigate this discrepancy between the two abundance estimates for CS in the hot core, we have simulated the spectrum which would be obtained from the hot core in a $34''$ gaussian beam, for comparison with the single-dish spectrum of the CS(1–0) presented by Hasegawa et al. (1984). The peak in the resulting spectrum is only 1 K, and shows that CS emission from the hot core is weaker than either the ridge or the plateau when observed with these large beams. Given that the CS(1–0) line is optically thick, the CS(5–4) observed by Blake et al. (1987) has an even higher optical depth, and the 1 K line from the hot core would have been completely masked by the 20 K emission from the ridge; the hot core was too beam-diluted to have been identified as a separate component using a spectral decomposition technique.

Our new abundance measurement for CS in the hot core calls into question some of the details of the chemical sequences outlined by Blake et al. (1987) for Orion, particularly with respect to the sulphur chemistry. The low abundances of CS, SO, and SO_2 derived by Blake et al. for the hot core were interpreted as being caused by most of the sulphur remaining tied up in the cores of the dust grains, along with other refractory species such as silicon. However, the abundances of SO and SO_2 recently obtained from high-resolution measurements by Wright et al. (1996), of 5.4×10^{-8} and 5.7×10^{-8} respectively, are also somewhat higher than the upper limits reported by Blake et al. This suggests that beam-diluted SO and SO_2 emission from the hot core may have been hidden in a manner similar to the CS in those single-dish observations. Again, these new abundances are intermediate between those observed for the plateau region and the extended ridge.

Most of the models for sulphur chemistry which exist in the literature have been calculated assuming either cold molecular clouds with T = 10 to 50 K (e.g., Prasad & Huntress 1982; Millar & Herbst 1990) or the passage of a shock (Mitchell 1984; Leen & Graff 1988). In a region such as the hot core which has been passively heated to $\sim$ 200 K or more none of these models is applicable. The closest comparisons between the hot core observations and chemical models which can currently be made is with the post-shock equilibrium abundances for CS, SO, and SO_2, calculated by Pineau des Forêts et al. (1993) for temperatures up to 150 K and densities $n(\mathrm{H}) = 10^5$ cm^{-3}. These authors find that while the abundance of CS remains relatively constant as a function of temperature, the activation energy of 265 K for one of the important formation routes for SO, S + $O_2 \rightarrow$ O + SO, means that the abundance of both SO and SO_2 (which is formed from the further reaction of SO with O_2 or OH) steadily increases with temperature. These models do not reproduce the observations of the hot core, underestimating the abundances of all three molecules, but suggest that further modelling using higher temperatures and densities will be essential for explaining these data.

5. Conclusions

Images of the Orion-IRc2 region at $2''$ resolution in 43 GHz continuum and CS(1–0) emission have been obtained using the VLA. By removing uv spacings shorter than 40 kλ and imaging only structures less than $2.5''$ in size we find that unresolved continuum emission is associated with the previously known radio sources B and I. An extended component is also observed which peaks at source I rather than the hot core. We have investigated whether spectral line emission within our 50 MHz continuum channel can account for the extended structure, but conclude that it cannot. A comparison of the 43 GHz image with 22 GHz data indicates that it may be free-free emission from gas being ionized by source I; the HII region must have a high dust content to explain the derived emission measure compared to the infrared luminosity of the region. The location of the ionized gas closer to source I than the emission from either dust or molecular lines suggests that source I may have even more extreme excitation conditions than the hot core. This fits well with the results recently reported by Blake et al. (1996) where the hot core is being passively heated by source I and within the hot core the highest excitation temperatures are measured at smaller projected distances from I.

The CS(1–0) image shows that most of the compact emission is concentrated in the hot core. A peak line temperature of ~ 150 K is derived from these data, indicating that the CS(1–0) transition is optically thick. CS emission also arises from the compact ridge and the western clump, but no dense molecular gas was detected at the position of the Becklin-Neugebauer object. The CS is resolved into several distinct clumps, each of which can be identified with the single-dish components via the line width and centre V_{LSR} of their spectra. A smooth velocity gradient is observed along the ridge of material from the hot core to the compact ridge in which mainly oxygen-bearing molecules are usually observed. The western clump appears to comprise two velocity components, one of which may be redshifted gas associated with the outflow from source I.

The detection of significant CS emission in the hot core contradicts the upper limit for the CS abundance in this component derived by Blake et al. (1987) from a single-dish spectral line survey with $30''$ resolution. We estimate an abundance $X(\mathrm{CS}) = 1.2 \times 10^{-8}$ relative to H_2, which is lower than the value obtained by Blake et al. for the plateau, but higher than that obtained for the extended ridge. We conclude that the hot core component was too beam-diluted in the earlier single-dish survey, and was confused by the strong emission from the ridge. A comparison between the abundances of the sulphur-bearing molecules SO and SO_2 measured in the single-dish survey with those obtained on small scales by Wright et al. (1996) suggests a similar result. Existing models for sulphur chemistry do not extend to the conditions observed in the hot core ($n(\mathrm{H_2}) > 10^7$ cm^{-3},

T = 150 to 200 K), the closest being the chemical equilibrium models for post-shock gas calculated by Pineau des Forêts et al. (1993), which uses $n = 10^5$ cm^{-3} and temperatures up to 150 K. These models under-predict the abundances of CS, SO, and SO_2, compared with those measured in the hot core, and indicates that more extensive modelling is required to explain the observations.

We are particularly grateful to Lee Mundy for providing us with 22 GHz continuum images. We also thank John Richer for his careful reading of an earlier version of the text. CJC held a Janksy Postdoctoral Fellowship at the National Radio Astronomy Observatory in Socorro, New Mexico, during part of this work, and also acknowledges the support of an Advanced Fellowship from the UK Particle Physics and Astronomy Research Council.

Table 1. Properties of the CS clumps in the Orion-IRc2 region.

Clump	R.A. (1950) (h m s)	Dec. (1950) (° ′ ″)	approx. size ″ × ″	PA (°)	V_{LSR}[a] (km s^{-1})	ΔV[a] (km s^{-1})
1	05 32 47.12	−05 24 24.2	2.7 × 0.8	22 ± 7	4.9	5.4
2	05 32 47.05	−05 24 26.2	2.1 × 1.1	29 ± 11	5.8	8.0
3	05 32 46.99	−05 24 28.4	3.0 × 0.9	35 ± 11	7.5	3.3
4	05 32 46.77	−05 24 31.3	3.8 × 2.0	39 ± 49	7.7	4.2
5	05 32 46.80	−05 24 24.4	1.9 × 1.0	135 ± 10	3.7	7.9
6	05 32 46.64	−05 24 21.4	2.2 × 0.7	121 ± 11	10.2	8.3

[a]Derived from single Gaussian fit to spectrum. May not be appropriate for clumps 5 and 6 (see text).

REFERENCES

Anthony-Twarog, B. J., 1982, AJ, 87, 1213

Blake, G. A., Mundy, L. G., Carlstrom, J. E., Padin, S., Scott, S. L., Scoville, N. Z., Woody, D. P., 1996, ApJ, in press

Blake, G. A., Sutton, E. C., Masson, C. R., Phillips, T. G., 1987, ApJ, 315, 621

Briggs, D. S., 1995, PhD Thesis, New Mexico Institute of Mining and Technology

Caselli, P., Hasegawa, T. I., Herbst, E., 1993, ApJ, 408, 548

Chandler, C. J., De Pree, C. G., 1995, ApJ, 455, L67

Chernin, L. M., Wright, M. C. H., 1996, ApJ, 467, 676

Downes, D., Genzel, R., Becklin, E. E., Wynn-Williams, C. G., 1981, ApJ, 244, 869

Dougados, C., Léna, P., Ridgway, S. T., Chistou, J. C., Probst, R. G., 1993, ApJ, 406, 112

Genzel, R., Reid, M. J., Moran, J. M., Downes, D., 1981, ApJ, 244, 884

Genzel, R., Stutzki, J., 1989, ARA&A, 27, 41

Gezari, D. Y., 1992, ApJ, 396, L43

Hansen, S. S., Johnston, K. J., 1983, ApJ, 267, 625

Hasegawa, T., et al., 1984, ApJ, 283, 117

Hermsen, W., Wilson, T. L., Bieging, J. H., 1988a, A&A, 201, 276

Hermsen, W., Wilson, T. L., Walmsley, C. M., Henkel, C., 1988b, A&A, 201, 285

Hollenbach, D., Johnstone, D., Lizano, S., Shu, F., 1994, ApJ, 428, 654

Leen, T. M., Graff, M. M., 1988, ApJ, 325, 411

Mangum, J. G., Wootten, A., Plambeck, R. L., 1993, ApJ, 409, 282

Masson, C. R., Claussen, M. J., Lo, K. Y., Moffet, A. T., Phillips, T. G., Sargent, A. I., Scott, S. L., Scoville, N. Z., 1985, ApJ, 295, L47

Masson, C. R., Lo, K. Y., Phillips, T. G., Sargent, A. I., Scoville, N. Z., Woody, D. P., 1987, ApJ, 319, 446

Masson, C. R., Mundy, L. G., 1988, ApJ, 324, 538

Menten, K. M., Reid, M. J., 1995, ApJ, 445, L157

Mezger, P. G., Henderson, A. P., 1967, ApJ, 147, 471

Migenes, V., Johnston, K. J., Pauls, T. A., Wilson, T. L., 1989, ApJ, 347, 294

Millar, T. J., Herbst, E., 1990, A&A, 231, 466

Mitchell, G. F., 1984, ApJ, 287, 665

Murata, Y., Kawabe, R., Ishiguro, M., Morita, K.-I., Hawegawa, T., Hayashi, M., 1992, PASJ, 44, 381

Pauls, T. A., Wilson, T. L., Bieging, J. H., Martin, R. N., 1983, A&A, 124, 23

Pineau des Forêts, G., Roueff, E., Schilke, P., Flower, D. R., 1993, MNRAS, 262, 915

Plambeck, R. L., Wright, M. C. H., Carlstrom, J. E., 1990, ApJ, 348, L65

Plambeck, R. L., Wright, M. C. H., Mundy, L. G., Looney, L. W., 1995, ApJ, 455, L189

Poynter, R. L., Pickett, H. M., 1985, Applied Optics, 24, 2335

Prasad, S. S., Huntress, W. T., 1982, ApJ, 260, 590

Tatematsu, K., et al., 1993, ApJ, 404, 643

Wilner, D. J., Wright, M. C. H., Plambeck, R. L., 1994, ApJ, 422, 642

Wright, M. C. H., Plambeck, R. L., Mundy, L. G., Looney, L. W., 1995, ApJ, 455, L185

Wright, M. C. H., Plambeck, R. L., Wilner, D. J., 1996, ApJ, 469, 216

Wright, M., Sandell, G., Wilner, D. J., Plambeck, R. L., 1992, ApJ, 393, 225

Wright, M. C. H., Vogel, S. N., 1985, ApJ, 297, L11

This preprint was prepared with the AAS LaTeX macros v4.0.

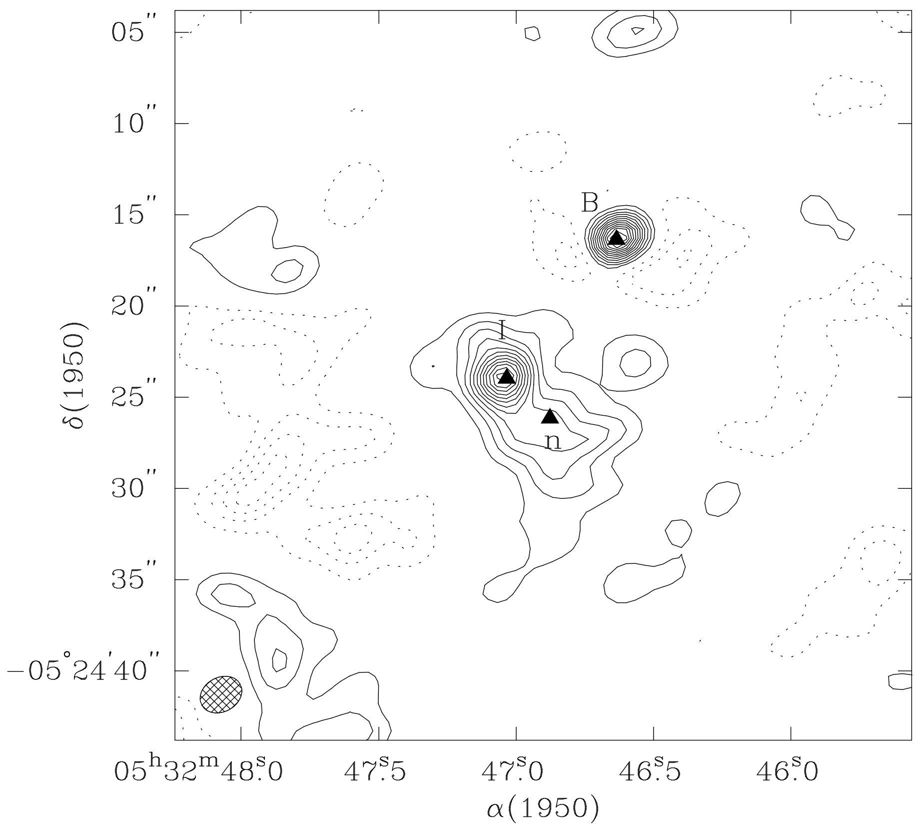

Fig. 1.— Continuum image of the Orion-IRc2 region obtained at 43.3 GHz using the VLA. The synthesised beam is 2.″38 × 1.″87 at P.A. −60° and is plotted as a hatched ellipse in the lower left corner. The filled triangles denote the positions of radio sources I, B and n. The contours are at approximately 3σ intervals of 1.5 mJy beam^{-1}.

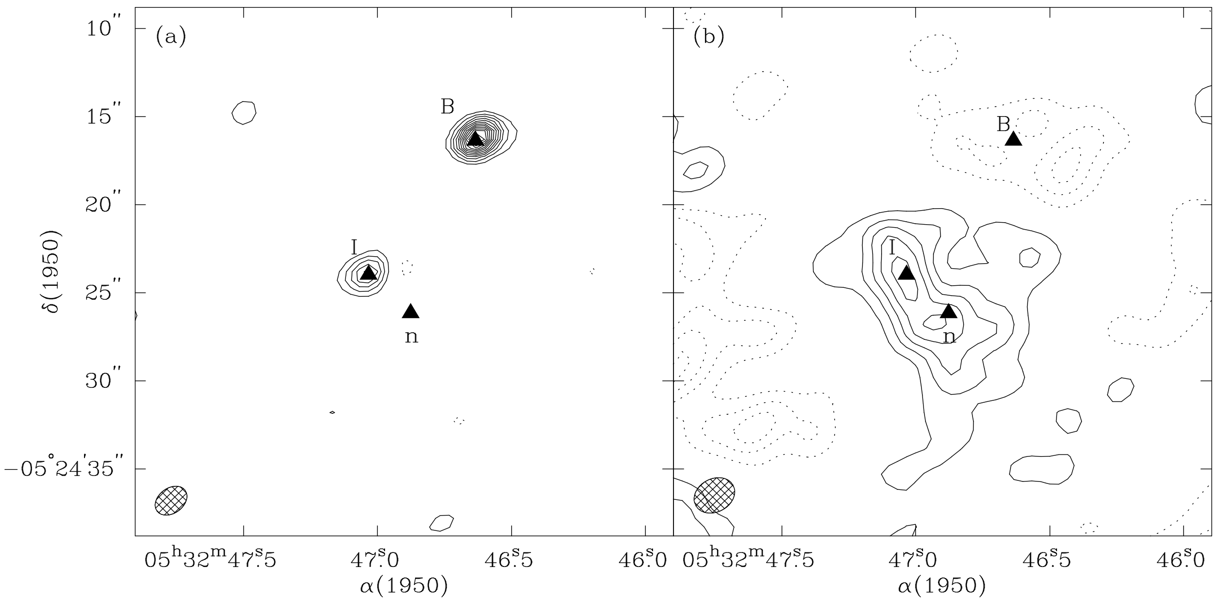

Fig. 2.— *a.* 43 GHz continuum image of Orion-IRc2 made with only those *uv* spacings longer than 40 kλ. The resulting synthesised beam, plotted in the lower left of the image, is $1''.96 \times 1''.41$ at P.A. $-52°$. The contour levels are at intervals of 2.0 mJy beam^{-1}. *b.* 43 GHz continuum image obtained after subtracting point sources at I and B from the *uv* data. The synthesised beam is the same as in Figure 1. Contours are equally spaced at intervals of 1.5 mJy beam^{-1}.

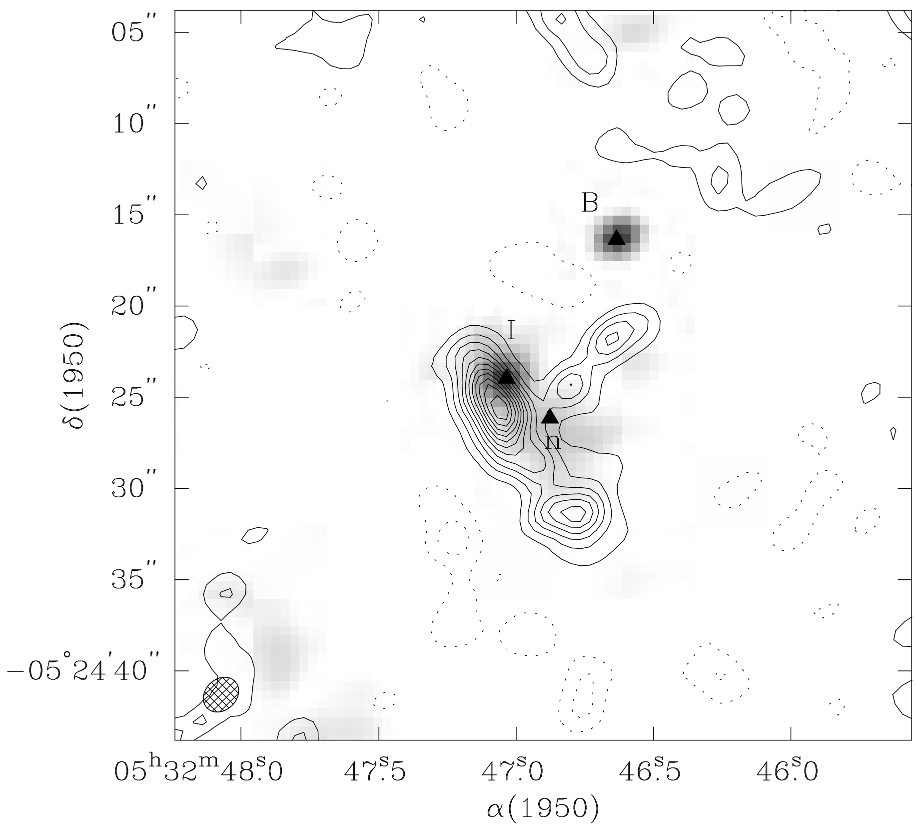

Fig. 3.— Contours of CS(1–0) emission integrated between $V_{\rm LSR} = -2.0$ and 13.6 km s^{-1}, overlaid on a greyscale representation of the 43 GHz continuum from Figure 1. The synthesised beam is 2.″11 × 1.″69 at PA −46°. The contour levels are spaced at 3σ intervals of 0.37 Jy km s^{-1}.

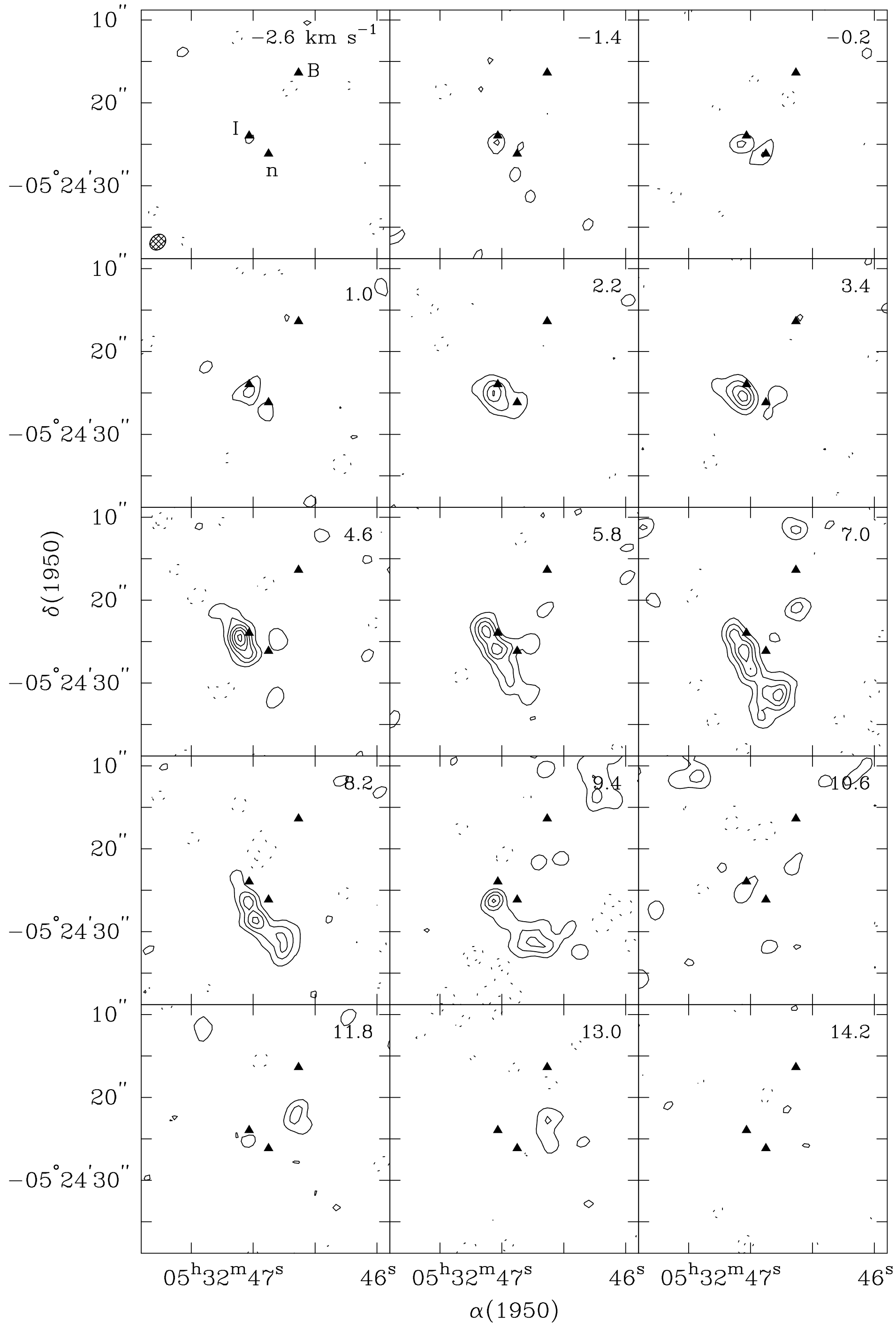

Fig. 4.— Channel maps of the CS(1–0) emission in Orion. The LSR velocity is given at the top right of each panel, km s^{-1}. Contours are spaced at 3σ intervals of 99 mJy beam^{-1} (14 K).

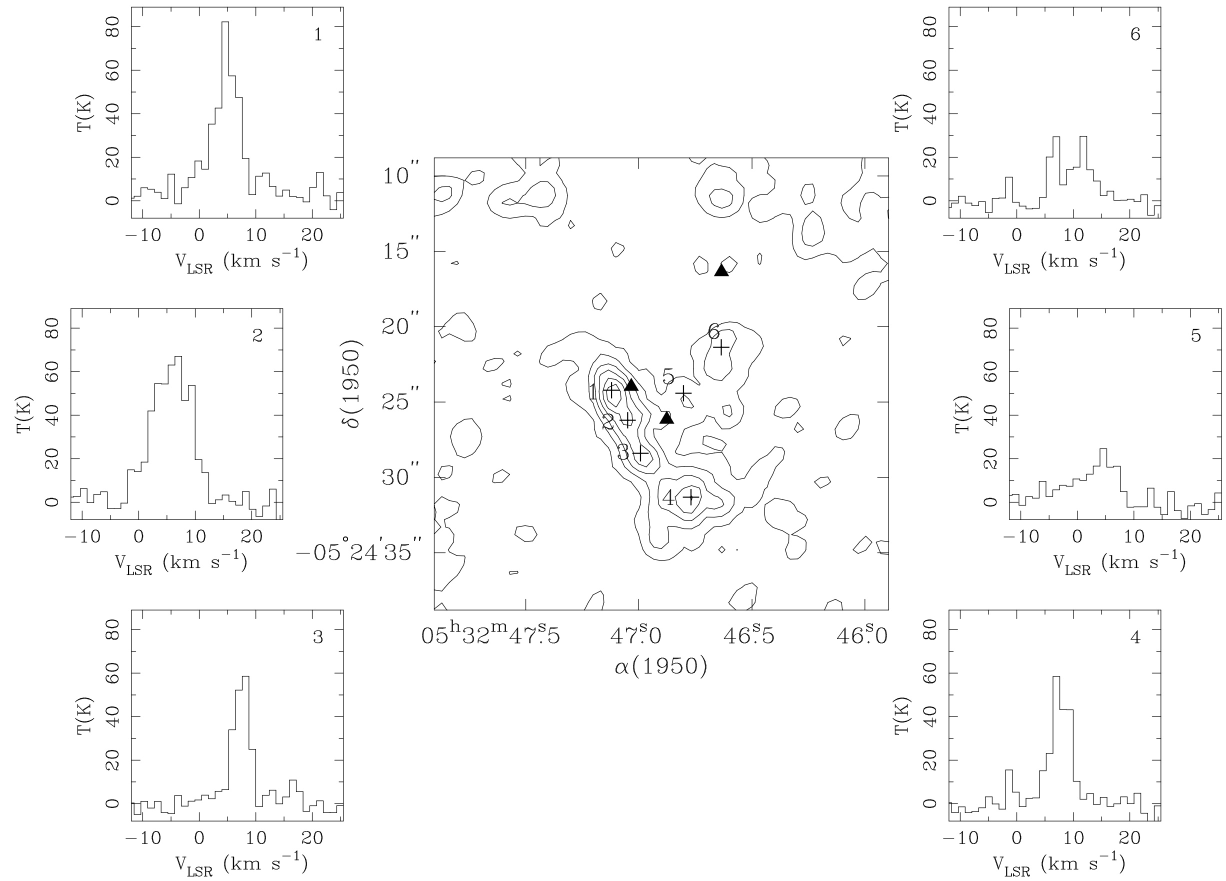

Fig. 5.— Contours of peak beam-averaged brightness temperature, T_B, with the locations of clumps 1–6 marked as crosses. The positions of radio sources B, I and n are also plotted as filled triangles. Contours are equally spaced at intervals of 13 K. A spectrum of each clump is also displayed, showing the LSR velocities and line widths typical of the hot core (clumps 1 and 2), and the compact ridge (clumps 3 and 4). Clump 5 has a blueshifted wing possibly associated with the outflow from source I, and the clump 6, the western clump, has two distinct velocity components.

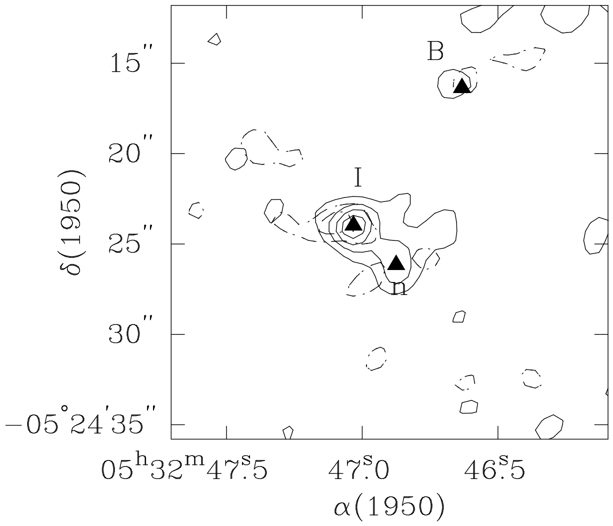

Fig. 6.— High-velocity CS(1–0) emission associated with source I. The blueshifted emission (solid contours) is integrated between $V_{\rm LSR}$ = −13.9 and -2.0 km s^{-1}, and the redshifted emission (dot-dash contours) is integrated between 20.7 and 32.7 km s^{-1}. Contours are spaced at 2σ intervals of 0.24 Jy km s^{-1} in both images. The continuum has not been subtracted from the spectral line data, and the emission at source B is consistent with continuum emission. At sources I and n, however, the contribution from the continuum is negligible.

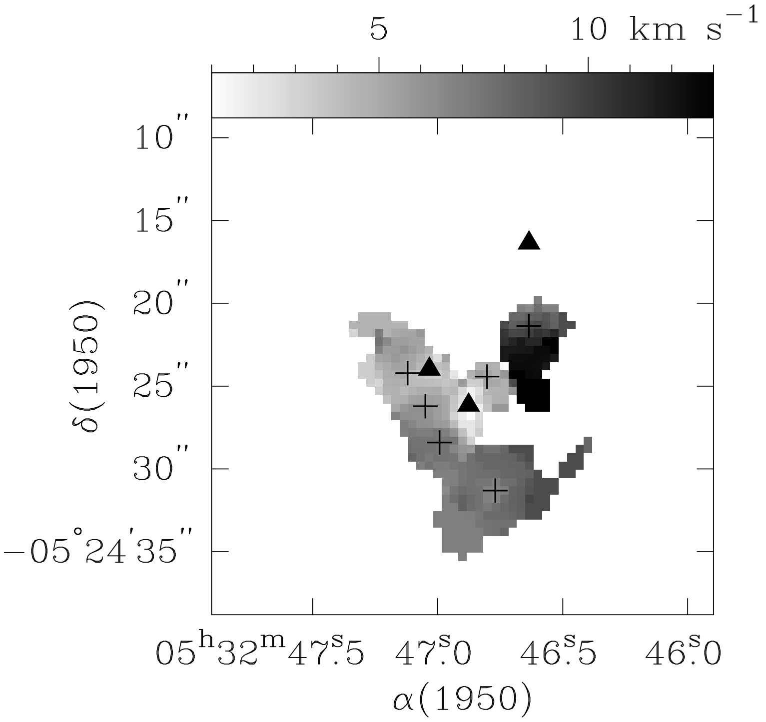

Fig. 7.— Greyscale image of the intensity-weighted mean velocity across the CS-emission region. Clumps 1–6 are marked as crosses, and sources B, I and n are filled triangles.